Post-Flight Attitude Reconstruction for the Shuttle Radar Topography Mission

Edward Wong*, William Breckenridge, Dhemetrios Boussalis,
Paul Brugarolas, David S. Bayard*, John Spanos, Guru Singh
Jet Propulsion Laboratory, California Institute of Technology,
4800 Oak Grove Drive, Pasadena, CA 91109

ABSTRACT

The Shuttle Radar Topography Mission (SRTM) is the first mission to provide high accuracy near-global topographic coverage of the Earth's land surface using a long-baseline interferometry approach. It uses a synthetic aperture radar instrument to produce a digital elevation map with 16 m absolute vertical height accuracy at 30 meter postings. The mission involves a large space structure (60 meter mast) deployable from the Shuttle payload bay and requires precision attitude and position determination to arc-minute and millimeter levels. Onboard flight sensors include electro-optical metrology sensors, a target tracker, a star tracker, gyros, and GPS receivers. On the first day of flight, system identification of the mast frequency and damping was conducted in near real-time on the ground using flight sensor telemetry data for proper tuning of the Shuttle attitude control system. Post-flight reconstruction of the attitudes and positions of the outboard and inboard antennas over a nine-day period was conducted. A description of the ground software system architecture and the data processing methodology is provided. Implementation and results of various attitude reconstruction methods for minimizing the radar height errors involving large space structures, such as optimizing structural and time misalignments, data interpolation, time synchronization, estimator and model tuning, and nonlinear filtering, are described.

1. Introduction

The Shuttle Radar Topography Mission (SRTM) is a project jointly sponsored by NASA and the National Imagery and Mapping Agency (NIMA) with the objective of generating high accuracy global topographic maps. SRTM was launched on February 11, 2000 for an 11-day Space Shuttle mission. It provided coverage of 80% of the earth's land surface based on data acquired during flight. It had collected enough radar measurements and onboard sensor data for a digital model of the Earth that would satisfy the requirements of 16 meter absolute vertical height accuracy, and 30 meter postings. These results will provide significant improvement over existing global topographic maps. The SRTM coordinates and in-flight antenna orientation are shown in Fig 1.1.

The SRTM architecture consists of a 60 meter mast and supporting mechanisms to deploy an "outrigger" (outboard) radar antenna. The main (inboard) antenna remains inside the Shuttle bay. The attitude determination system provides algorithms for the necessary baseline metrology, and determines attitudes and positions of the radar antennas to accuracy of arc-minutes and milli-meter to support mission operations and topography data processing. Platform position and velocity determination is provided by an onboard GPS system. Detailed description of the GPS data processing is not included in this paper.

Member AIAA

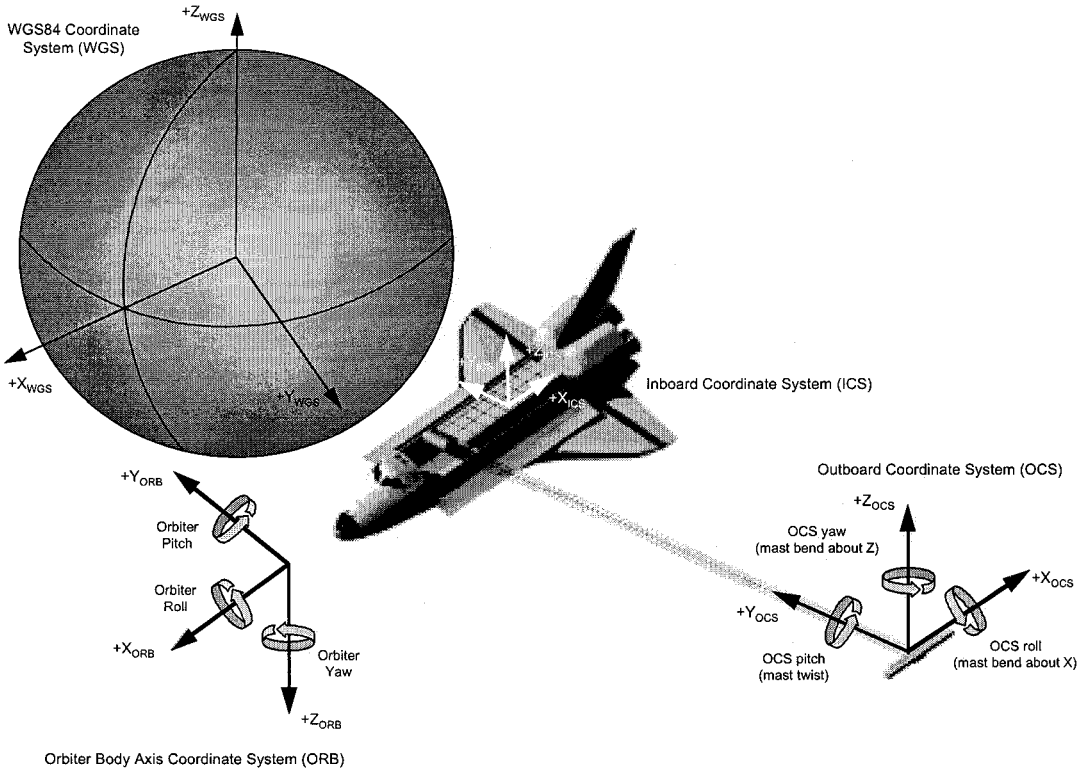

Fig 1.1 SRTM coordinates and flight configuration

2. Architecture for Attitude Reconstruction

The SRTM attitude determination system configuration is depicted in Figure 2.1. The knowledge of the antennas has two primary components: the inboard radar antenna attitude and position, and the outboard antenna attitude and position relative to the inboard radar antenna. The inboard attitude was measured by a Star Tracker Assembly and an Inertial Reference Unit (IRU). The star tracker is the Lockheed Martin Autonomous Star Tracker (AST-201). It has a 8.8° x 8.8° field-of-view and employs a star catalog containing 16,000 stars. It performs autonomous acquisition with no a-priori attitude knowledge and typically tracks 30-50 stars. It operates at rates of 0.5°/s and degraded accuracy for rates as high as 2°/s. The tracker produces quaternions representing its inertial attitude at 2 Hz. The IRU is a Teledyne Dry Rotor Inertial Reference Unit (DRIRU-II) which outputs angular increments also at 1 Hz [3]. The IRU measurements can further refine the attitude estimate during data processing. Note that the star tracker, IRU, and GPS sensors are necessary because the Shuttle guidance and navigation systems cannot provide the required accuracy and also significant thermal distortions are expected between the Shuttle guidance platform and the SRTM inboard antenna.

To determine the outboard antenna's attitude and position relative to the inboard antenna, a target tracker was used to continuously view the outboard from its inboard location. The tracker, developed by JPL in the 1980's to serve as a high precision star tracker for pointing applications, was flown on the Shuttle twice (Astro-1 and Astro-2) and had demonstrated sub-arcsecond accuracy in-flight. Significant modifications were made to accommodate the SRTM architecture, such as adding a new corrective lens to focus at a distance of 60 meters, and optical filters to reduce straylight. The tracker tracked three red (635 nm) light emission diode (LED) targets located on the outboard antenna. The LEDs were mounted on graphite-epoxy "stalks" and separated by 1 meter both laterally and in line of sight. The target tracker produced centroid information in charged couple device (CCD) line and pixel coordinates on all three

targets at a rate of 8-9 Hz, but only the first four samples of each second were used, producing a non-uniform update rate.

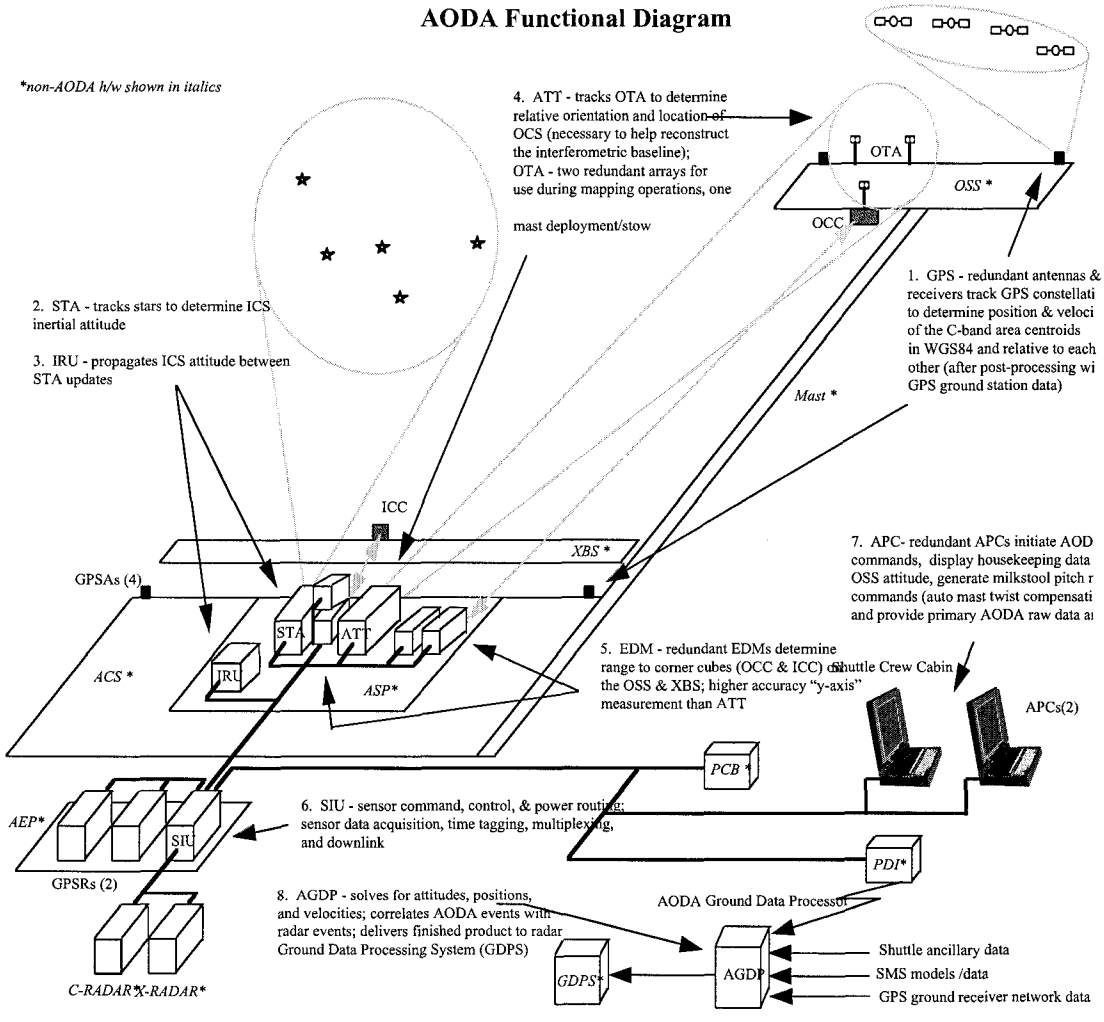

Fig 2.1 SRTM Attitude Determination Configuration

Because the target tracker had intrinsically poor accuracy in determining its line-of-sight component (derived from comparing two LED position measurements), it was necessary to add additional metrology instruments capable of measuring the range from the inboard to the outboard antenna to high accuracy. A commercially available surveying rangefinder, known as an Electronic Distance Meter (EDM) (Leica-Wild DI2002) was used. The EDMs had a fairly small field-of-view (approximately 1.7 mrad), and their target was an array of corner-cube reflectors (40 cm diameter) located on the inboard edge of the outboard antenna. Although rotations of the outboard antenna produced errors in the range solution, the resulting range accuracy was still better than 2 mm.

All the sensor measurement data collected in the 11-day mission was stored in the hard drives of two laptop computers' located in the Shuttle's crew cabin, and transferred once the Shuttle has landed for post-flight attitude reconstruction. Partial sensor data was downlinked in real-time during the mission for a quick system verification and mast system identification.

The ground attitude reconstruction software processed telemetry data output by all the sensors above collected over a 9-day period during the 11-day mission. Other data files processed simultaneously were the Shuttle thruster firings telemetry, the ground processed GPS data, and the structural deformation data modeled from temperature measurements. The architecture of the ground software is depicted in Fig 2.2. The system identification software will output the identified modal frequencies and damping in a separate data file. The remaining ground software will provide a file containing the attitude and position estimates of the two antennas and their covariances in various coordinate systems at 4 second intervals.

3. Attitude Reconstruction Requirements

In the first 12 hours of the mission, the attitude determination operations were very closely linked with the deployment of the mast, alignment of the antennas, and optimization of the Shuttle attitude control system. There were close interactions between ground operators and the astronaut crew (via the laptop computers) during this period. For safety reasons, successful deployment of the mast was verified before proceeding with the mapping phase of the mission. If one or more latches do not snap into place completely even when the mast was completely extended, the mast would be susceptible to collapse in response to Shuttle thruster firings. The Shuttle stayed in free drift in a stable gravity-gradient attitude during mast deployment verification. Onboard estimation of deployed mast tip position and attitude errors enabled the astronaut crew and ground teams to verify mast integrity before enabling the Shuttle attitude control system.

Due to practical difficulties of performing precision modal tests of a 60 meter deployed mast structure in a 1-g environment, the pre-flight estimates of mast modal frequencies are expected to be accurate to within 20%. Since notch filter settings in the Shuttle's attitude control system were selected to reduce mast response, errors in pre-flight estimates could lead to excessive attitude control response and fuel consumption, thereby shortening the length of the mission. In-flight modal identification tests were performed to improve the knowledge of the mast frequencies and damping, and allow for optimization of the Shuttle attitude control system. It turned out that this in-flight identification was crucial because the passive damper at the root of the mast failed to function in flight.

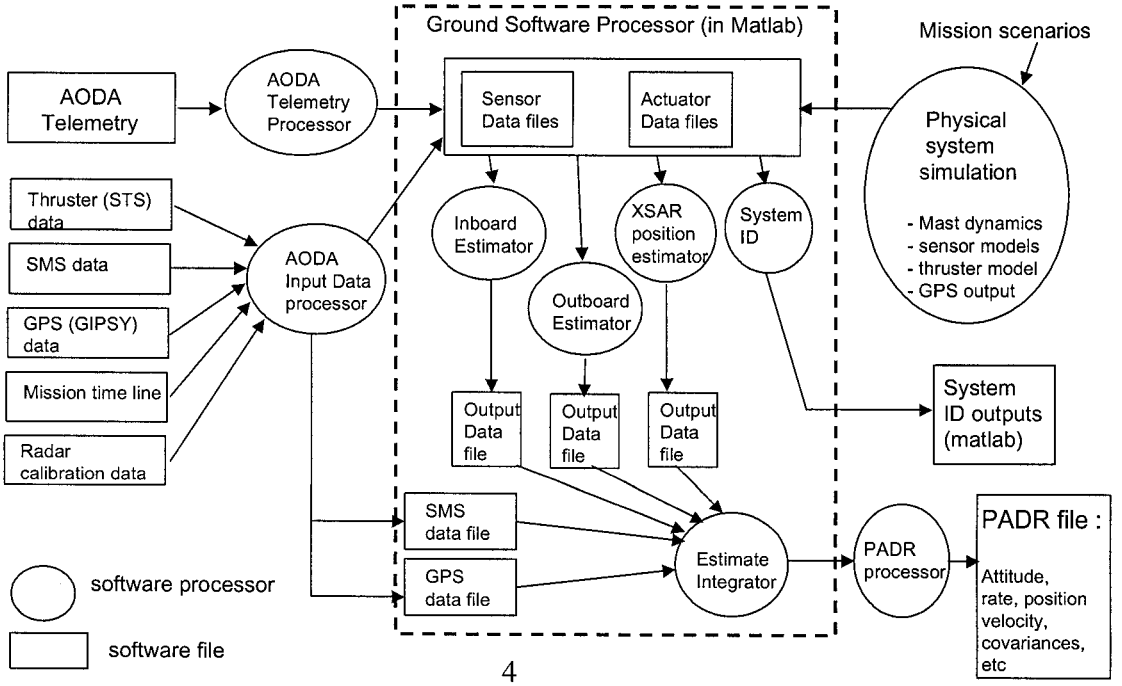

Fig 2.2 Attitude Reconstruction Software Architecture

The errors in baseline angle, baseline length, and platform height had significant impact on the total SRTM radar mapping accuracy. The baseline roll angle, in particular, is one of the largest error sources. The requirement is to provide estimation of the interferometric baseline length, attitude, and position at the accuracy of 2 mm, 9 arcsec, and 1 m levels, respectively, throughout the entire mission whenever sensor telemetry data is available. Large systematic error biases, such as sensor-to-platform misalignment, or star tracker optical bias, could be removed by radar calibrations. Such calibration was accomplished by performing radar ground data-takes periodically during the mission over well-surveyed land sites, but the majority took place over the ocean.

4. Mast Structure dynamics

The mast, developed by AEC-Able, was a composite structure composed of graphite epoxy longerons and battens with steel fittings and titanium cables. When deployed, formed a rigid structure with primary modal frequencies on the order of 0.1 hz. The mast was designed to provide minimal thermally-induced distortions, allow deployment and retraction (20 min each time), and was capable of being jettisoned in an emergency.

The mass of the outboard antenna is 128 Kg, and the mast is around 15 Kg. The combined mast and outboard antenna represent a large moment-arm on the Shuttle ordinarily not designed for. The mast alone had very little inherent damping, resulting in the need to add viscous damper struts at the root to prevent resonant instability in response to the Shuttle attitude control system. Such viscous dampers failed to operate once the mast was deployed. It was evidenced by the observed motion of the outboard before and after the dampers were uncaged. Furthermore, since the SRTM mapping geometry requires that the mast be maintained at a 45° angle with respect to nadir, the resulting gravity-gradient torque was near the worst. A continuous-thrust cold gas propulsion system was added to the outboard antenna to compensate for this torque and reduce Shuttle fuel consumption. It was also evident that such cold gas thrusters did not produce thrust as expected. It was decided in flight that the Shuttle attitude control deadband be widened (from 0.5 to 1.0 deg) in order to conserve Shuttle fuel and preserve the mission duration.

Mast pointing is affected by several factors. Gravity unloading, launch shifts, and pre-flight assembly and alignment errors resulted in a quasi-static pointing bias. In-flight thermal distortions of the mast and antenna structures (bending and twisting) created pointing errors with time-constants of tens of minutes. Also, the mast responded dynamically to the Shuttle attitude control system thruster firings and astronaut crew activities. Mast bending would cause relative misalignment between the two antennas (e.g., a 3 cm tip translation results in a 0.1° antenna misalignment). Hence, mast pointing errors impacted the attitude determination and radar sensor's capability in both target acquisition and tracking.

5. Identification of Mast Frequency and Damping from Flight Data

The system identification was needed for fine tuning certain notch filters in the attitude controller of the space shuttle, and for verifying deployment and appropriate operation of the SRTM mast dampers. For the former, it is required to estimate the dominant modal frequencies below 0.5 Hz for the mast, while the latter requires approximate determination of the damping coefficients.

Two operations were conducted immediately after deployment of the mast. The first was performed with the dampers caged (low-damping) and the second with the dampers un-caged (high-damping). Each experiment will result in a data set of, approximately, fifteen minutes duration. It was this operation that uncovered the failure of the viscous dampers.

The System Identification Approach

Identification of the mast frequencies and damping may be accomplished utilizing target tracker (ATT) or IRU measurements. It is, however, preferable to use the ATT since it observes only the in-board to out-board relative motion.

The ATT is an optical sensor, similar to a star tracker, observing three light sources (LED) on the Optical Target Assembly (OTA) which is mounted on the out-board antenna. The ATT processes four exposure frames per second and reports the target image position in CCD coordinates (pixels). The image coordinates are denoted by $\{u_i(t_k), v_i(t_k)\}$, $i = 1,2,3$ and t_k is the time tag of the processed frame. By combining all frames six time histories (two for each LED) are constructed and processed by an estimator to generate three displacements and three rotations.

The system identification package consists of the following algorithms:

1. A data processing algorithm to convert target tracker data to three-axis (small) angles, and,
2. the Eigensystem Realization Algorithm with Data Correlation (ERADC)

ERADC processes signals representing the impulse response of the system and generates a minimal realization $\{A, B, C, D\}$, that is a linear time-invariant system with impulse response identical to that given as input to the identification algorithm. The choice of ERADC over a simple PSD was based on the fact that this method will result in a good estimate of the frequencies and damping, as well as to a state-space model. The performance criterion is the error between the ATT generated signals and the corresponding impulse response of the realized system obtained by MATLAB simulation.

To experimentally generate the necessary data, the structure must be excited by input (force) signals approximating an impulse. In the case of SRTM, the system identification experiments were conducted by first disabling the STS attitude control and then exciting the mast by firing the vernier thrusters in pulses of 1.25 sec duration. This was the shortest possible pulse duration available at that time, with the consequence that, under the impulse response approximation, ERADC will yield accurate results for modes up to 0.2 Hz.

Figure 5.1 shows the results of one of the experiments. The measurement was the time histories of the image coordinates of LED 2 converted into displacements in the orbiter X-Z plane. This motion captures the mast oscillations of interest. It is clear that the impulse response of the identified system is a good approximation of the actual response. The identified modal frequencies are 0.091 Hz and 0.132 Hz with damping ratios of 0.015 and 0.028, respectively. Figure 5.2 shows the PSD plots for the two signals.

Further careful analysis of the measurements, together with measurements from the IRU and STA has shown that the mast exhibits non-linear and time-varying behavior. Specifically, the damping has non-linear characteristics, while the frequency of oscillation varies with amplitude and angular acceleration. The system identification results, however, are well within the bounds defined by these perturbations.

Another significant observation was that results obtained with the mast root dampers un-caged (high-damping) actually indicated lower damping than that with the dampers caged. This was a first indication of the dampers had failed.

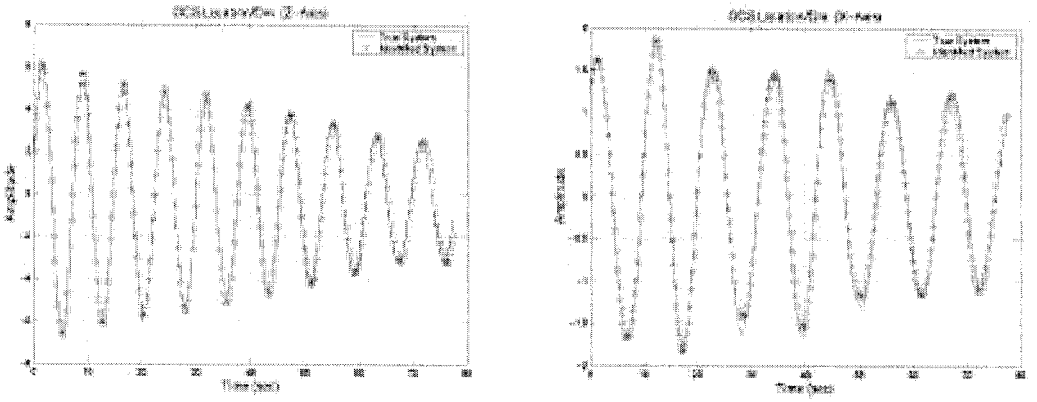

Figure 5.1: Impulse responses of the true (measured) and identified systems

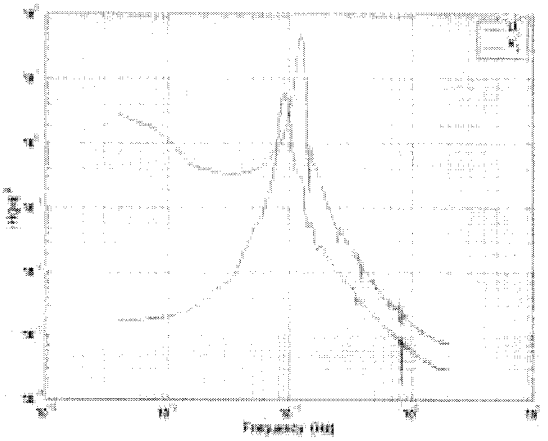

Figure 5.2: PSD of the impulse response of the identified system.

6. Inboard (main) Antenna Attitude Reconstruction

The in-board attitude estimator generates estimates of the orientation of the STA coordinate system relative to the inertial reference frame J2000. The attitude is in the form of a quaternion representing the rotation from J2000 to STA. The in-board attitude estimator accepts inputs from the Star Tracker (STA) and the Inertial Reference Unit (IRU).

The STA utilizes an internal star catalog and software to generate the attitude of the STA coordinate system relative to J2000. The process is triggered in one-second intervals by an external sync pulse. During the following RTI (1 sec) the STA software processes two exposure frames and returns the attitude quaternion q_m (also interpreted as rotation from J2000 to STA) and the angular increment between this quaternion and the one corresponding in the first exposure frame. This provides the user with the capability of reconstructing 2 Hz measurements in case they are needed.

The IRU is sampled at a rate of 1Hz and provides incremental angles obtained from three two-axis rate-integrating gyroscopes (DRIRU II). Each sense axis continually provides a pulse count proportional to the integrated rate. A pulse counter accumulates the algebraic sum of the pulses every RTI and then resets. Thus, the resulting net pulse count over the one-second interval when multiplied by the appropriate scale factor yields the incremental angle for this particular sampling interval.

Post-mission analysis revealed several problems related to attitude sensors as well as the on-board data acquisition process which dictated substantial modifications of the in-board data pre-processing and estimator algorithms. Specifically, the first run of the estimator with actual mission data resulted in unexpectedly high residuals, a fact that motivated an in-depth search to determine the error sources. The following major error contributors were identified:

1. Corrupted STA measurements, eventually leading to elimination of, approximately, 30% of the star tracker data.
2. Time alignment error between the STA quaternion and IRU measurement resulting from the fact that the STA window tracking software assumed constant velocity even in regions of high angular acceleration. Introducing a second-order extrapolation scheme to synchronize the two measurements reduced the effect of this error component.
3. The unexpected appearance of an aliased mode due to the low IRU sampling rate. This led to the introduction of a complementary low-pass filter to de-emphasize gyro participation at low frequencies. The new configuration may be viewed as a "two-pole" extended Kalman filter.
4. Frame misalignments which caused the appearance of orbit and 100 second periodic error components of substantial amplitude in the residual. Late delivery of the STA hardware did not allow for accurate optical alignment, consequently, a-priori knowledge of the relative frame orientation was based on drawings and associated tolerances. This motivated an elaborate task of determining the non-orthogonal coordinate transformation between the two frames. It was found that, for some of the IRU sense axes, the alignment error was as high as 0.4 degrees.

After applying the above modifications, the RMS value of the estimator residual improved by one order-of-magnitude. The following is a brief description of the processes associated with the in-board attitude estimator:

Data Pre-Processing:

Time tags, IRU and STA measurements are inspected for consistency. Bad data points are identified and marked to be excluded by the filtering process. The STA reported quaternion is corrected for velocity aberrations.

The Linearized State Equations

Let q and $\hat{q}$ be the true and estimated attitude quaternions, respectively, related by

$$q = \Delta q \hat{q}$$

where Δq represents the correction defined by

$$\Delta q = q\hat{q}^* = \begin{bmatrix} \frac{1}{2}\Delta\theta \\ 1 \end{bmatrix}$$

Furthermore, let Δb represent a perturbation in the gyro drift rate. Then a linear, discrete-time state-space representation may be obtained as

$$x_k = \Phi_{k-1} x_{k-1} + w_{k-1}$$
$$\Phi_k = I + A(\Delta\hat{\theta}_k^g, T_k)$$
$$A(\Delta\hat{\theta}_k^g, T_k) = \begin{bmatrix} -\Delta\hat{\theta}_k^g & -T_k \\ 0 & 0 \end{bmatrix}$$
$$x_k = \begin{bmatrix} \Delta\theta_k \\ \Delta b_k \end{bmatrix}$$

The Observation

The true, measured, and estimated quaternions denoted by q, q_m and $\hat{q}$, respectively, are related by $q_m = \Delta q_m \hat{q}$, $q_m = \Delta q_v q$, and $q = \Delta q \hat{q}$, where Δq_m, Δq_v and Δq are the measurement residual, measurement error due to noise and the estimation error, respectively. Then it can be shown that

$$\delta\theta_k^m = Hx_k + v_k$$

with the independent measurement generated by

$$\delta\theta_k^m = 2S(q_m^k \hat{q}_{k|k-1}^*)$$

where $H = I_{3\times 6}$, and $S = I_{3\times 4}$.

Propagation Between Updates (Prediction)

The filtered incremental angle is: $\Delta\hat{\theta}_k^g = \Delta\theta_k^g - \hat{b}_{k-1} T_k$, where delta θ^g is the gyro measured angle, and state is propagated by:

$$\hat{x}_{k|k-1} = \Phi_{k-1}\hat{x}_{k-1|k-1}; \quad \hat{x}_{k-1|k-1} \equiv 0$$

This relation is presented for completeness only since it, obviously, implies that $x_{k|k-1} \equiv 0$. The covariance matrix is propagated by

$$P_{k|k-1} = \Phi_{k-1} P_{k-1|k-1} \Phi_{k-1}^T + Q_{k-1}$$

and the predicted quaternion, under small angle approximation, is evaluated by:

$$\hat{q}_{k|k-1} = \begin{bmatrix} \frac{1}{2}\Delta\hat{\theta}_k^g \\ 1 \end{bmatrix} \hat{q}_{k-1|k-1}$$

The observation updates are as follows:

$$\hat{x}_{k|k} = \hat{x}_{k|k-1} + K_k(\Delta\theta_k^m - H\hat{x}_{k|k-1})$$
$$K_k = P_{k|k-1}H^T(HP_{k|k-1}H^T + R_k)^{-1}$$
$$P_{k|k} = (I - K_kH)P_{k|k-1}(I - K_kH)^T + K_kR_kK_k^T$$
$$\hat{q}_{k|k} = \Delta\hat{q}_k\hat{q}_{k|k-1}$$
$$\hat{b}_{k|k} = \hat{b}_{k|k-1} + \Delta\hat{b}_{k|k}$$
$$\Delta\hat{q}_k = \begin{bmatrix} \frac{1}{2}\Delta\hat{\theta}_{k|k} \\ 1 \end{bmatrix}$$

The update without a measurement and the reset state are:

$$P_{k|k} = P_{k|k-1}$$
$$\hat{q}_{k|k} = \hat{q}_{k|k-1}$$
$$\hat{b}_{k|k} = \hat{b}_{k|k-1}$$
$$\hat{x}_{k|k} = 0$$

The performance of the estimator is summarized in the figures presented in the following. Figure 6.1 shows the measured (blue dots) and estimated (continuous line) attitude quaternion. The blue dots at 0 amplitude correspond to the rejected data points. Figure 6.2 shows the IRU generated and estimated incremental angles (blue dots and continuous red line, respectively). The estimated biases are shown in Figure 6.3. Note that after compensating for the frame alignment errors, the bias estimates mainly reflect the gyro drift rates. Figure 6.4 represents the estimation a-priori residuals. In this particular case the RMS values of the residuals for the X, Y and Z axes are 1.88, 2.27 and 18.18 micro-radians, respectively.

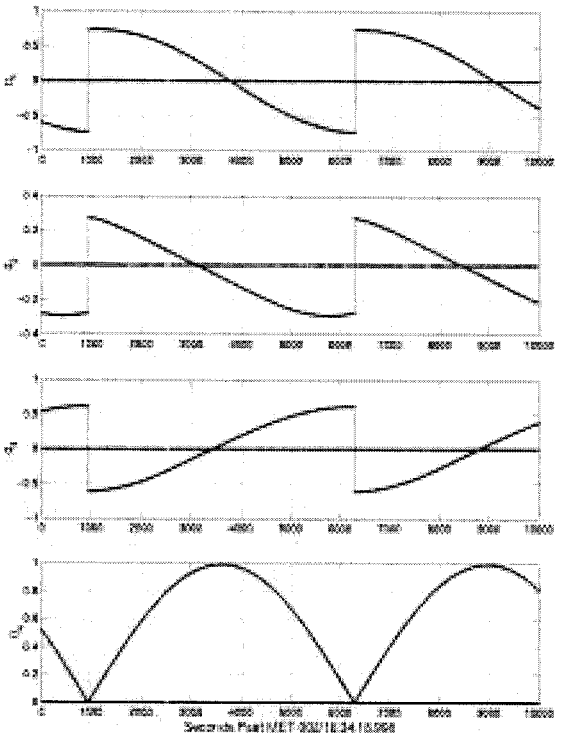

Figure 6.1: Measured and estimated quaternion.

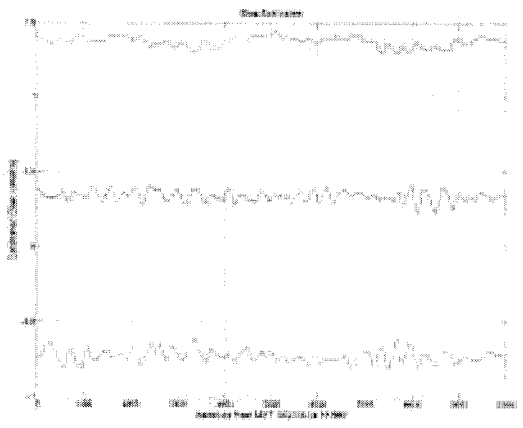

Figure 6.3: Bias estimates.

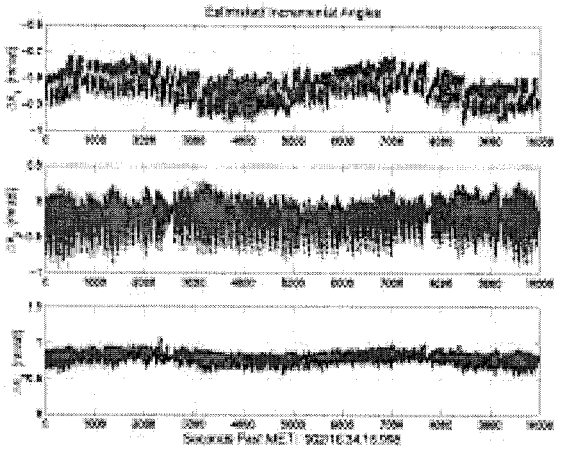

Figure 6.2: Measured and estimated incremental angles.

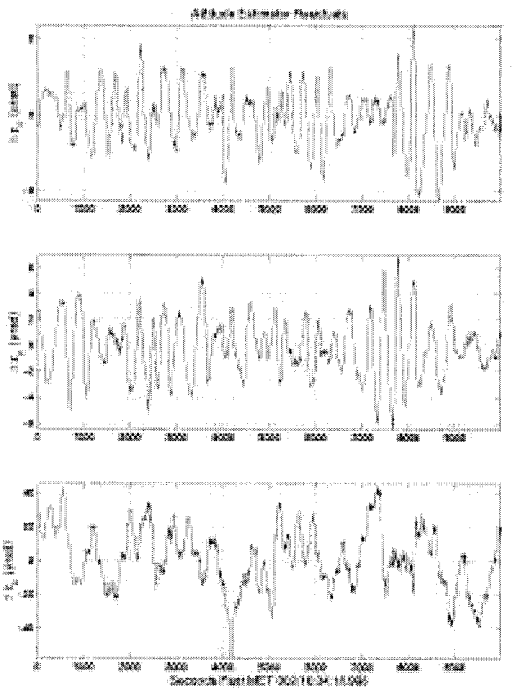

Figure 6.4: Estimator residuals.

Speed-of-light Correction

A speed-of-light (the aberration correction) correction is also applied to the attitude estimate in the inboard attitude estimator. The purpose of this analysis is to verify the correctness (magnitude and direction) of the aberration correction. The primary difference between the verification analysis here and the original implementation is the SRTM orbit data. Previous analysis used an analytic approximation whereas the verification analysis uses the orbit based on the GPS data (187359.37 MET : 187359.37 MET+15000 seconds).

Four time-histories are shown in Fig. 6.5. The top-left figure depicts the angle between the STA-Z axis (the bore-sight) and the orbital velocity vector. This should be close to 75° and it is (this is to verify that correct orbit is being used). Slight variation from the expected 75° line is due to small mismatches in the GPS data time-tags. The top-tight figure depicts the actual correction needed to the non-corrected attitude (blue solid line) as well as the theoretical limit (red dashed line) based strictly on the angle between the earth helio-centric velocity and the STA-z axis. Actual corrections ranged from 20 μradians to 115 μradians.

The bottom-right plot in Fig. 6.5 depicts the angle between the STA-z axis and the SRTM helio-centric velocity (solid line) and the magnitude of this velocity vector (dashed line). The angle variation is orbit-periodic and it varies between 10°-100°. The total correction shown in top-right figure is a function of the angle and the magnitudes depicted in the plot on the bottom right.

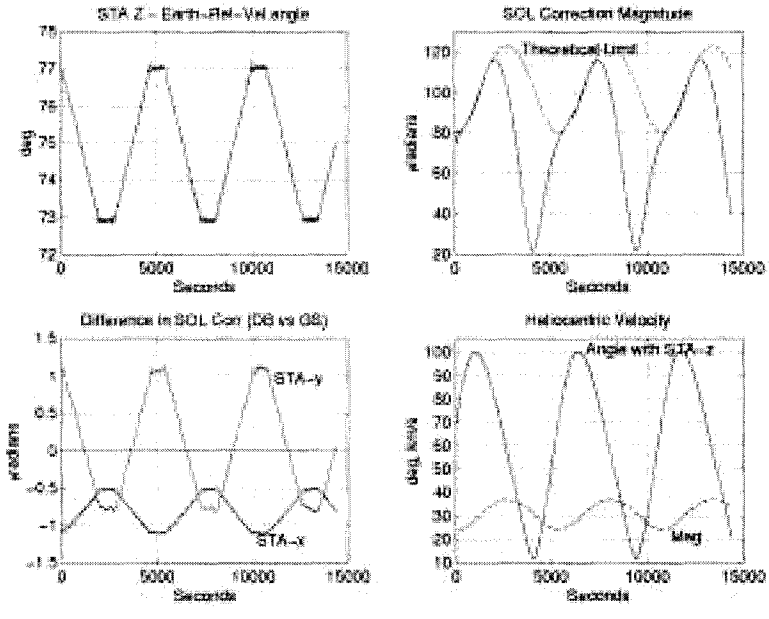

Fig 6.5 Speed of Light Correction

The bottom-left plot compares the SOL-corrected attitude evaluation in the verification analysis with the previous results. No correction is needed about the roll axis (z). The difference in corrections in the other two direction is 1.1 μradian or less.

The difference in corrections in the two different analyses is less than 1.5 μradians (total), which when compared with the total correction (20-115 μradians) implies that the SOL correction applied in the original analysis is correct in size as well as direction.

7. Estimation of Inboard Attitude Frame Alignment

This section focuses on estimating the alignment between the Gyro and Star Tracker frames in support of the inboard attitude estimator.

Background

The relevant frames for calibration are shown in Figure 7.1. The main objective of the alignment effort is to estimate the transformation M between the STA cube frame and STA (body) frame. The transformation from the STA to ICS frame will then be deduced by extracting and inverting the rotational part of M.

The signals from three chosen gyros are stacked into the vector θ_g, which represents the integrated rate (i.e., the incremental angle) measured along each gyro axis. This measured incremental angle is transformed into body coordinates using,

$$\theta(t_k) = M_0 G^{-1}\ \theta_g(t_k)$$

Here, $\theta(t_k)$ denotes the incremental change in attitude in body coordinates as measured by the gyros over the time interval from t_{k-1} to t_k; the quantity $G^{-1} \in R^{3\times 3}$ is a general nonorthogonal matrix which maps gyro measurements to the STA cube frame; and the matrix M_0 is an initial estimate of the desired alignment matrix. The matrix M_0 was obtained using the same method as will be discussed below, except using only the Day 2 data set.

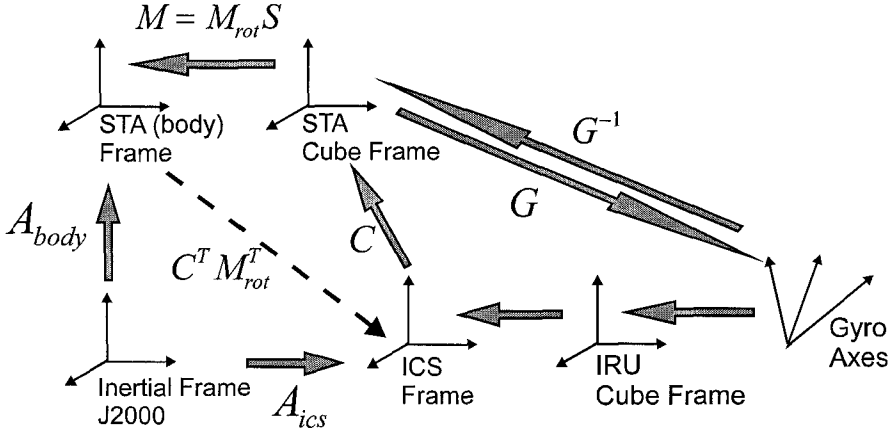

Figure 7.1: Relevant frames for calibration

Calibration Data

The frame alignment matrix M is calibrated by comparing the incremental angle θ from the gyro, with the incremental angle ϕ produced by time-differencing the time and acceleration corrected star tracker quaternion. Specifically, ϕ is extracted from the following expression,

$$q_T(t_k) \cdot q_T^*(t_{k-1}) = \begin{bmatrix} \phi/2 \\ 1 \end{bmatrix}$$

where, $q_T(t_k)$, $q_T^*(t_{k-1})$ denote the corrected star tracker quaternion measurements at times t_{k-1} and t_k, respectively, and the superscript symbol "*" denotes quaternion conjugation.

The data used for alignment purposes was taken by combining measurements taken on 3 different days into a single estimation problem. Specifically, one 14400 second (i.e., 4 hours) data segment is taken from each of Day 2, 4, and 9 giving a total of $14400 \times 3 = 43200$ seconds for estimation.

Calibration Model

The model used for calibration is given by,
$\phi_\ell(t_k) = (I + \delta M)\theta_\ell(t_k) + b_\ell + c_\ell t_k + v_\ell(t_k)$

The quantities ϕ and θ are the incremental angles measured from the STA and IRU, respectively; and $\delta M \in R^{3\times3}$ is the alignment matrix with 9 independent entries, allowing for all rotation, scale factors and nonorthogonality errors to be calibrated. The vector quantities $b_\ell, c_\ell \in R^3$ are used to fit the gyro bias and bias drift, respectively, over each of the ℓ'th days where $\ell = 2,4,9$. This gives a total of $9 + 2 \times 3 \times 3 = 27$ parameters to be estimated by the calibration procedure.

The quantity $v_\ell(t_k)$ is the measurement noise associated with $\phi_\ell(t_k)$. From a separate analysis the covariance was found as,

$$Cov[v_\ell(t_k)] = V = (6\text{e-}6)^2 \cdot \begin{bmatrix} 1 & 0 & 0 \\ 0 & 1 & 0 \\ 0 & 0 & 10 \end{bmatrix}$$

Lowpass Filter Data Pre-processing

It was found essential to sharply lowpass filter all data before using it for alignment purposes. This was an important "lesson learned" for this mission.

For filtering purposes, a bicausal tenth-order Butterworth filter having a cutoff of .03 Hertz was used to filter both sides of the calibration equation, giving the filtered estimation model,

$$\tilde{\phi}_\ell(t_k) = (I + \delta M)\tilde{\theta}_\ell(t_k) + b_\ell + c_\ell \tilde{t}_k + \tilde{v}_\ell(t_k)$$

where $\tilde{\phi}_\ell, \tilde{\theta}_\ell, \tilde{t}_k, \tilde{v}_\ell$ denote the lowpass filtered time signals. The lowpass filter profile is superimposed on a plot of the STA Y axis PSD in Figure 7.2 using Day 2 data. As desired, the filter rejects all modal energy in the vicinity of .14 Hz and above while retaining informative low frequency energy.

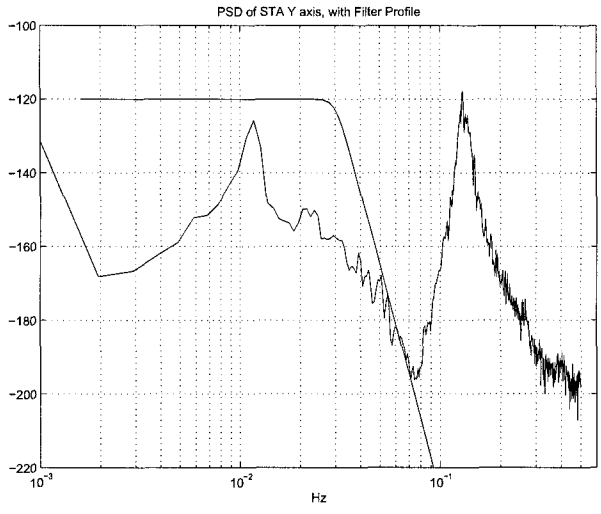

Figure 7.2: Butterworth lowpass filter profile superimposed on STA Y-axis incremental angle PSD

Estimation Approach

The filtered estimation model is rearranged into the form,

$$y_\ell(t_k) = \delta M\tilde{\theta}_\ell(t_k) + b_\ell + c_\ell\tilde{t}_k + \tilde{v}_\ell(t_k), \quad k = 0,\ldots,N(\ell)$$

where $N(\ell)$ is the number of time points in the data segment for the ℓ'th day, and the quantity $y_\ell(t_k)$ is defined as,

$$y_\ell(t_k) = \tilde{\phi}_\ell(t_k) - \tilde{\theta}_\ell(t_k)$$

The rearranged filtered expression is linear in the parameters. A standard minimum-variance approach is used to estimate the parameters making use of the noise covariance V given earlier[5] .

Frame Calibration Results

The results of the alignment calibration are summarized below.

From Figure 7.1 one can rewrite the transformation from gyro axes to STA (body) frame as,

$$\theta(t_k) = MG^{-1}\theta_g(t_k)$$

where,

$$M = (I - \delta M)M_0$$

Here, M is a single matrix which contains all of the alignment corrections to the original gyro-to-body mapping G^{-1}. It can be calculated by using M_0 and the estimated δM to give,

$$M = \begin{bmatrix} 9.992086962691312e\text{-}001 & -4.605097509962209e\text{-}003 & 1.227024002373918e\text{-}003 \\ -6.003031327817818e\text{-}003 & 9.935815792834721e\text{-}001 & 3.794052912266092e\text{-}003 \\ -2.239768511054158e\text{-}003 & 4.916862806748802e\text{-}003 & 1.001977309930110e{+}000 \end{bmatrix}$$

Indications from the error analysis are that the first two rows of M are estimated to better than 30 urad accuracy, while the last row (associated with the degraded STA axis) is good to 300 urad.

STA to ICS Alignment

The inboard attitude estimator produces the attitude A_{body} in the STA frame. If M in Figure 7.1 were a pure rotation, the conversion to attitude A_{ics} in the ICS frame would be straightforward. However, since M is not a pure rotation, the rotational part will be extracted by solving the optimization problem,
$\min_{M_{rot}} \; || M_{rot}G^{-1} - MG^{-1} ||_f^2$

subject to,
$M_{rot}^T = M_{rot}^{-1}$

where $|| \cdot ||_f$ denotes the Frobenious norm. Mathematically, this problem finds the rotation M_{rot} which in cascade with G^{-1}, best explains the MG^{-1} product.

Solving the optimization problem gives the rotation matrix,

$$M_{rot} = \begin{bmatrix} 1 & 7.345391660150975e\text{-}004 & 1.176126994958482e\text{-}003 \\ -7.345391660150975e\text{-}004 & 1 & 3.656588691648919e\text{-}003 \\ -1.176126994958482e\text{-}003 & -3.656588691648919e\text{-}003 & 1 \end{bmatrix}$$

The inverse rotation M_{rot}^T is applied to all attitude estimates from the inboard estimator, to map them from the true body frame to the ICS frame, i.e.,
$A_{ics} = C^T M_{rot} A_{body}$

Height Improvement

Results summarized here indicate misalignments on the order of 1/3 degree. The alignment correction had a significant effect on improving mission performance, dropping vertical height errors from about 6.4 to 3.1 meters RMS.

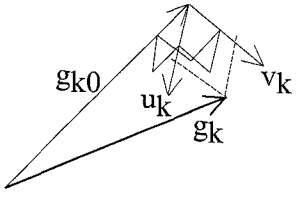

Alignment Estimation via Parameter Optimization

A parameter optimization approach is adopted to estimate the non-orthogonality among the three (nominally orthogonal) IRU axes and the mis-alignment between the IRU frame and the STA frame. A total of six parameters are to be estimated. Rather than model the mis-alignments and the non-orthogonalities in the

traditional manner, the approach perturbs each IRU axis in the two orthogonal directions (i.e. the two directions orthogonal to the nominal IRU sensing axis). This yields six parameters (3×2) and simultaneously captures the two effects to be estimated. The orientation of the perturbed k^{th} IRU sensing axis (g_k) is shown with respect to the non-perturbed axis (g_{k0}) in the figure on the left. Here g_{k0} is the nominal orientation of the k^{th} IRU axis in STA coordinates. The perturbation is achieved by moving in the orthogonal sub-space spanned by unit vectors (u_k, v_k). There are many choices for the (u,v) basis. Any choice must satisfy:

$$g_{k0} \bullet u_k = 0, \quad g_{k0} \bullet v_k = 0, \quad u_k \bullet v_k = 0, k = 1, 2, 3.$$

The (u,v) basis for each of the three IRU axes is computed once and fixed thereafter. Therefore if g_{k0} is the mis-aligned k^{th} IRU orientation in the STA frame, the aligned orientation can be expressed as:

$$g_k = g_{k0} + \theta_{uk} u_k + \theta_{vk} v_k; k = 1, 2, 3.$$

The angles θ_{uk} and θ_{vk} are expected to be small. There are six such angles to be estimated.

A very simple gradient-based search algorithm is used in estimated these parameters. The cost to be minimized is the inboard estimator residual RMS values about the STA-y axis over some fixed time. The terrain height estimates are most sensitive to this component of the residual. In the current implementation of the inboard estimator, two estimator passes are required for an "estimator run". Numerical evaluation of the gradient of the cost with respect to the six parameters therefore requires 12 additional passes for each set of candidate parameter vector [θ_{u1}, θ_{v1}, θ_{u2}, θ_{v2}, θ_{u3}, θ_{v3}]. At each iteration the solution proceeds in a direction which opposes the gradient. Search proceeds in small steps (proportional to the norm of the gradient) until the gradient vector norm becomes smaller than some prescribed value. The "optimal" parameter set [θ_{u1}, θ_{v1}, θ_{u2}, θ_{v2}, θ_{u3}, θ_{v3}] is found to be:

```
-6.45875, -8.45358, 13.4007, 0.0198659, -7.83571, -5.29801
```

Which implies a certain non-orthogonality and mis-alignment. The associated "misalignment" matrix is found to be

```
[ 1.000062116348557e+00 -2.158924603500850e-03
8.173104033721398e-03
 -7.808544170118168e-03  9.951976157501580e-01
5.117145702678157e-03
 -5.380402430661195e-03  1.209149799467973e-02
1.005106696709761e+00 ]
```

Use of this misalignment / non-orthogonality matrix lowers the inboard estimator residuals about STA-Y axis from 8.55 μrad to 5.89 μrad (1-sigma). No change was observed in the resilduals about the other two axes. The residuals (X, Y) time histories for a 4-hour period are ahown below. The plots on the left depict the X,Y residuals before mislaignment/non-orthogonality compensation. The plots on the right depict the post-compensation time histories.

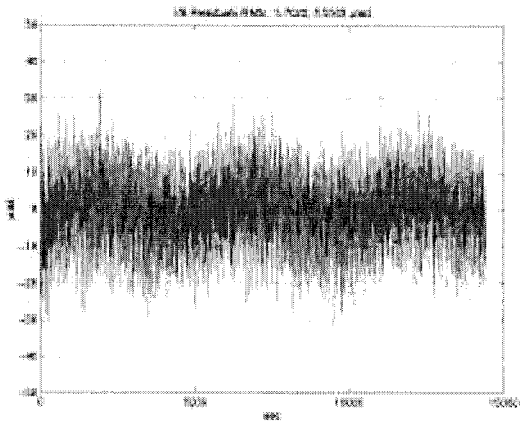

Fig. 7.3 Residuals before compensation

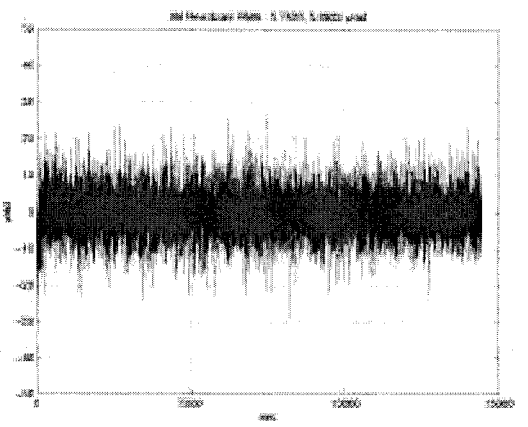

Fig 7.4 Residuals after compensation

Clearly, the misalignment compensation lowers the Y residuals, primarily by removing the ~100 second signature (pseudo-rigid body mode) from the residuals in the plots on the left. This is more clearly seen in Fig.7.5 which show a 500 second segment of the time history. The plot on the top has accounts for misalignments. The remaining motion (~7-8 second period) belongs to the dominant roll-bending mode of the mast.

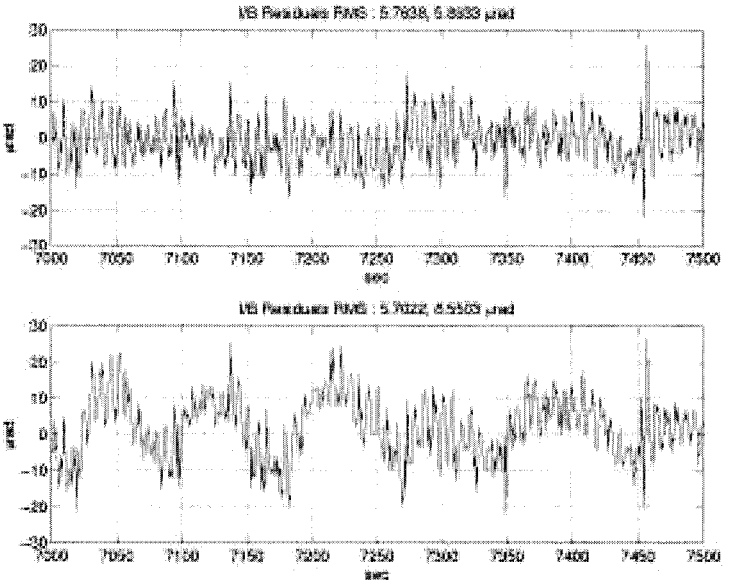

Fig. 7.5 Residual RMS

8. Outboard Antenna Relative Attitude and Position Reconstruction

The post-flight determination of position and attitude of the Outboard antenna with respect to the Inboard antenna was done by the outboard estimator. The outboard estimator design was presented in Ref [1]. In this section, we will briefly review it and emphasize the post-flight tuning of the estimator. This

estimator used measurements from the ASTROS Target Tracker (ATT) and an Electronic Distance Meter (EDM), and it was implemented as a discrete time Kalman filter.

The state of the filter was chosen to include 6 biases, 10 modal states, and 1 time latency state. The bias states (3 for position, 3 for orientation) estimate misalignments, launch shifts, mast deployment errors, nonlinear sticktion, and thermal distortions. These states do not have dynamics but we assign them some process noise to track slow changes due to thermal distortions, and sticktion of the roll bending mode.

The modal states are the magnitudes and rates of the 5 lower frequency flexible modes of the 60 m boom. These are the first and second roll and yaw bending modes and the twist mode. The dynamics for each mode are modeled as second order systems, where the mode shapes were taken from a NASTRAN model of the Shuttle with the SRTM payload (boom deployed, no viscous dampers), and the frequency and damping of each mode were estimated post-flight from the flight data. The first roll bending mode showed some nonlinear behavior, its frequency was amplitude dependent. A second order polynomial fit was used to model this behavior. Process noise in the rate states were used to account for variations in the frequencies and dampings, and inaccuracies on the mode shapes.

The latency state estimates an internal time-varying latency in the EDM, which is not included in the measurement time-tag. This latency state does not have any dynamics but it has a small process noise to account for variations in the latency.

Collected time histories of the Shuttle Vernier thrusters were used as the excitation for the Kalman filter dynamics.

The Kalman filter was formulated in the predictor-corrector as follows.

$$\hat{x}(k+1\,|\,k+1) = \hat{x}(k+1\,|\,k) + K(k+1)r(k+1\,|\,k)$$

$$\hat{X}(k+1\,|\,k+1) = [I - K(k+1)H(k+1)]\hat{X}(k+1\,|\,k)[I - K(k+1)H(k+1)]^T + K(k+1)V(k+1)K(k+1)^T$$

where, the estimator gain and the innovation process are defined as:

$$K(k+1) = \hat{X}(k+1\,|\,k)H^T(k+1)\left(H(k+1)\hat{X}(k+1\,|\,k)H(k+1)^T + V(k+1)\right)^{-1} \quad \text{for } k=0,1,2,\ldots$$

$$r(k+1\,|\,k) = z(k+1) - H(k+1)\hat{x}(k+1\,|\,k)$$

The outboard estimator was tuned based on feedback from radar calibration on height errors over ocean passes. As a result the estimator was tuned to mainly follow the measurements. The state equations were propagated from thruster firings times to measurement updates times dictated by the data. Because of inaccuracies in the mode shapes and models, the estimator was set to output estimates at ATT measurements times, and the thruster firing feed-forward term in the state equation was dropped, but it was used in the covariance propagation equations to accelerate the learning of the larger dynamics due to thruster firings.

Figures 8.1 and 8.2 show representative time histories of the position and orientation of the Outboard Coordinate System in the outboard antenna with respect to the Inboard Coordinate System in the Shuttle bay.

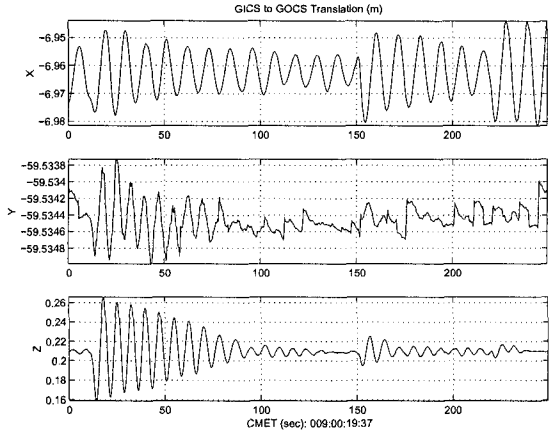

Figure 8.1 GOCS translation in GICS

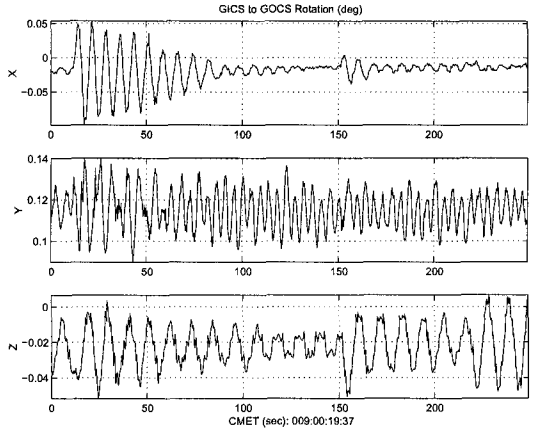

Figure 8.2 GOCS rotation in GICS (Euler Angles seq. 321)

9. Integrater of Attitude and Position Estimates

Data Record Integration

The objective of the integrater is to compile the Position and Attitude Determination Record (PADR). This file summarizes the position and attitude of the inboard and outboard radar antennas to be used to apply motion compensation in the interferometric processing of the radar data, which will produce the topographic maps (see [8,9] for more details). This file contains time histories at 4 Hz (synchronized with GPS time) of the positions of the antennas in the WGS84 frame, and orientations on the WGS84 and TCN frames, and relative position and orientation of the outboard with respect to the inboard.

The integration of estimates is done in the following steps:

1) Load input files.
   - Inboard estimates (estimates of the inboard attitude in J2000)
   - Outboard estimates (estimates of the outboard position and orientation with respect to the inboard)
   - Gipsy estimates (GPS based estimates of the spacecraft CG position and velocity in WGS84 [7])
   - Time correlation file (correlates GPS time with MET)
   - SDDR (Structure Deformation Data Record contains time histories of the thermal deformations between instruments)
2) Interpolate to 4 Hz (synchronized with GPS) using cubic splines.
3) Perform coordinate transformations to calculate PADR entries.
   - Static coordinate transformations.
   - J2000 to WGS84 calculated using SPICE with a high fidelity Earth rotation model.
   - WGS84 to TCN calculated using the method described in [6].
4) Perform SDDR corrections (if desired)
5) Save engineering PADR file.

Representative plots of some of the variables in the PADR file are given in figures 9.1 –9.5

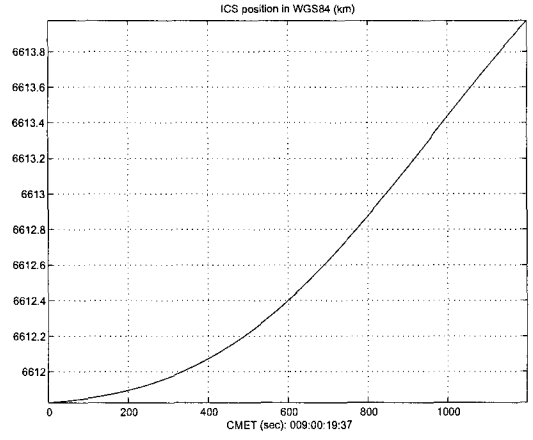

Figure 9.1 Magnitude GICS position in WGS84 (km)

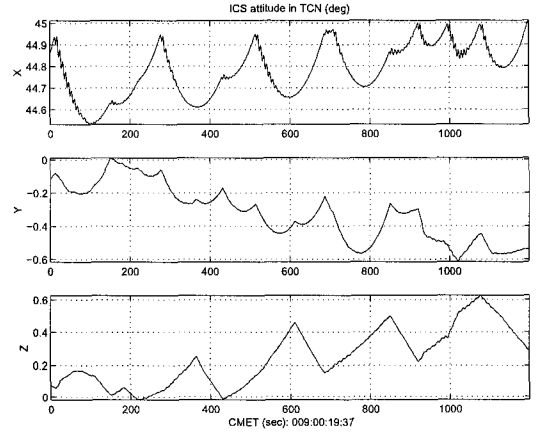

Figure 9.3 ICS attitude in TCN (Euler angle seq. 321)

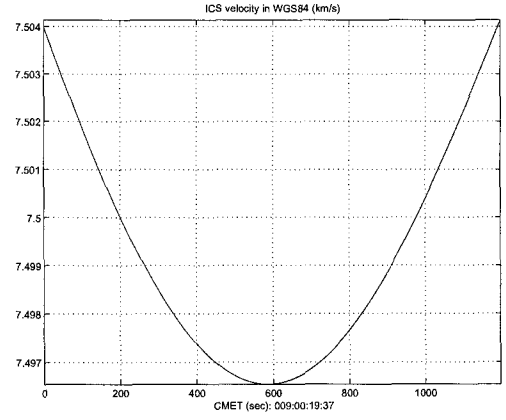

Figure 9.2 Magnitude GICS velocity in WGS84 (km/s)

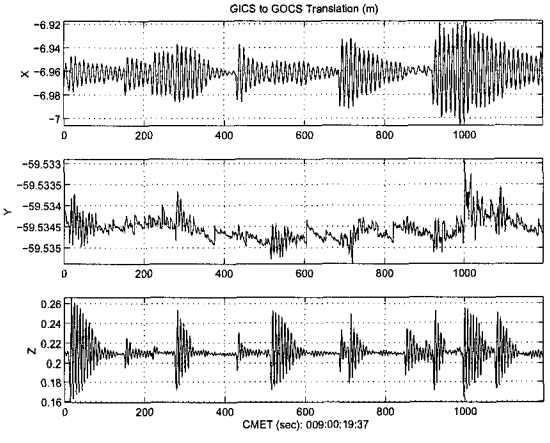

Figure 9.5 GOCS rotation in GICS (Euler Angles seq. 321)

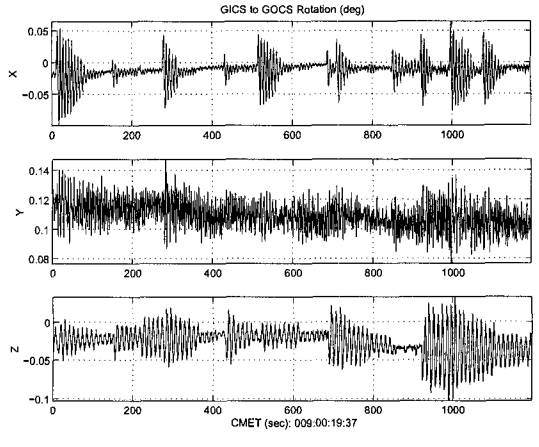

Figure 9.4 GOCS translation in GICS

Data Interpolation

At this time we turn our attention to the interpolation methods used by the Integrater. There are four instances in the data processing where interpolation is necessary. In each case there is a need to produce data on a uniformly spaced 4 Hz grid. First, due to its design the ATT is sampled at approximately 4 Hz but the samples are not evenly spaced. In this case the interpolation problem is simply to make the sampling grid uniform. Second, due to gyro under-sampling the inboard antenna attitude is estimated at the rate of 1 Hz with a clock having 1 millisecond variability. The task here is to interpolate the data to a uniform grid four times finer. Similarly, the GPS position and velocity as well as the quaternion describing the attitude of WGS in J2000 need to be up-sampled from 1 Hz to 4 Hz on the GPS clock.

From the numerous data interpolation methods available in the literature we considered cubic hermite polynomials, cubic splines, and sinc functions. Splines have continous second derivatives and are more accurate than hermite polynomials when the data come from a smooth function. Spline interpolation is also more accurate than sinc interpolation for data with very low frequency content. For data of high variability, sinc methods are far more accurate as they outperform splines by more than 2 orders of magnitude. However sinc methods are unable to deal with data sampled unevenly and this is one of the main reasons we selected splines for the interpolation problems cited above.

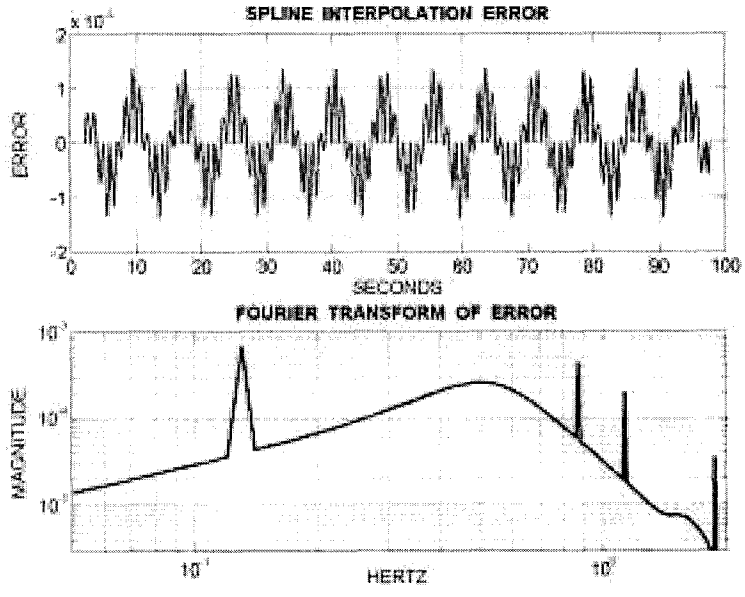

Figure 9.6. Spline interpolation error and its spectral distribution

Unfortunately the error introduced by interpolation is not limited to the frequencies of the signal. To better describe the error distribution we present the following simple example. A pure tone at 0.13 Hz representing the frequency of the boom roll mode is sampled at 1 Hz and then interpolated via cubic splines to 4 Hz. Figure 9.6 shows the temporal and spectral error from the interpolation process. We observe that the total error is approximately 0.13% and it is distributed almost evenly between the in-

band (frequency range of the signal) and out-band (higher frequency range). Specifically 0.07% error occurs at the frequency of the true signal (0.13 Hz) and 0.04%, 0.02% and 0.004% occurs in the out-band frequencies of 0.87 Hz, 1.13Hz, and 1.87 Hz respectively. This appears to be a non-negligible source of error and subsequently efforts were made to combine spline and sinc interpolants as well as spline interpolants and low pass filters in order to further reduce the out-band error.

10. Lessons Learned

The purpose of this section is to summarize the various lessons-learned as a result of the post-flight attitude reconstruction effort Much of the lessons are regarding the process of how things were done rather than the technology or data products themselves.

1. The cost constraint nature of the SRTM project had resulted in decisions being made quickly and without rigorous analysis. The understaffing/overwork resulted in a fairly rushed testing program in which several problems were overlooked.

2. SRTM could have benefited from a project system-level (combined Avionics and Radar) error budgets and calibration approach. Substantial post-flight effort was required to develop a calibration approach. The project could also have benefited from a project system level end-to-end validation & verification program including the combined Radar/Avionics hardware and ground-data processing algorithms.

3. The Star tracker was tested like standard star trackers which to date had been flown on deep space missions which didn't adequately simulate the unique SRTM/shuttle dynamics (60 meter mast induced base-body motions, etc). The star tracker spec should include raw star data (centroids) instead of an onboard computed quaternion. Having access to the raw observables is critical for unique applications such as SRTM. Our inability to access the raw observables (even in a snapshot fashion) meant we were blinded by the star tracker's internally computed error estimates (which masked the various problems) and limited our ability to do post-flight corrections.

4. Project System Engineering, Avionics, Analysis, and mechanical structure subsystems should have done a more rigorous analysis of the higher mast modes and the potential for aliasing. The analysis that was done suggested that the 2nd order modes had insignificant amplitudes. Since the first modes (around 0.1 Hz) were considered the drivers, they drove the design of the Avionics sensors (most notably the 1 Hz sampling of the IRU). The mast damper failure scenario was not analyzed in detail in advance, at least not with respect to sensor sample rates. Project system engineering should have worked harder to be able to sample IRU at 5-10Hz instead of 1 Hz (could have found a way around telemetry bandwidth limitation by compression or operational workarounds). Regarding review of the sample rates, there are two points to be made. Extensive discussion of EDM sample rates occurred pre-mission and resulted in a thorough revision of those requirements and a satisfactory resolution. However, discussions and independent reviews of IRU, star and target trackers sample rates (including outside organizations) did not raise any major concerns.

5. The magnitude of the target tracker S-curve effect was underestimated prior to launch, resulting in the need to perform post-mission calibration.

11. Conclusion

SRTM is the first mission to provide high accuracy near-global topographic coverage of the earth's land surface using a long-baseline (60 m) interferometry approach. The SRTM attitude reconstruction ground software system demonstrated the application of attitude determination techniques to interferometric baseline reconstruction. Post-flight reconstruction of the attitudes and positions of the outboard and inboard antennas over a nine-day period was conducted. A description of the attitude reconstruction software architecture and the data processing methodology is provided. Implementation and results of various attitude reconstruction methods for minimizing the radar height errors involving large space structures, such as optimizing structural and time misalignments, data interpolation, time synchronization, estimator and model tuning, and nonlinear filtering have been described. The results have demonstrated that the radar height errors are staying within the requirement of less than 3 meters.

Acknowledgments

Contributions or advice given to this paper by Harry Balian, F. Hadaegh, J. Alexander, Zahidul Rahman, R. Duren, and E. Litty, are appreciated. The research described in this paper was carried out at the Jet Propulsion Laboratory, California Institute of Technology, under contract with the National Aeronautic and Space Administration.

References

1. " Attitude Determination of the for the Shuttle Radar Topography Mission", E. Wong, W. Breckenridge, D. Boussalis, P. Brugarolas, AIAA Guidance, Navigation, and Control Conference, AIAA-99-3968, August 9-11, 1999, Portland, Oregon
2. "The SIR-C/X-SAR Synthetic Aperture Radar System", R. L. Jordan, B. L. Huneycutt, M. Werner, IEEE Transactions on Geoscience and Remote Sensing, Vol. 33, No. 4, July 1995
3. "Metrology, Attitude and Orbit determination for Spaceborne Interferometric Synthetic Aperture Radar." R. Duren, E. Wong, W. Breckenridge, S. Shaffer. C. Duncan, P. Solomon, and E. Tubbs. SPIE Aerospace Conference, Guidance and Navigation. 1998
4. "Applied System Identification", J-N. Juang, Prentice-Hall, 1994
5. G.A.F. Seber, *Linear Regression Analysis*. John Wiley & Sons, New York, 1977.
6. Improved Method for Calculating Exact Geodetic Latitude and Altitude. Isaac Sofair. Journal of Guidance, Control, and Dynamics. Vol. 20, No. 4, pp 824-826, July-August 1997
7. Precise Orbit Determination for the Shuttle Radar Topography Mission using a New Generation of GPS Reciever. W. Bertiger et al. In Proceedings of the ION GPS 2000 Conference. Salt Lake City, September 2000
8. Synthetic aperture radar interferometry. Rosen, P. et al. In Proceedings of the IEEE, Volume: 88 Issue: 3, March 2000
9. The SRTM topographic mapping processor. Hensley, S.; Rosen, P.; Gurrola, E. Geoscience and Remote Sensing Symposiun, 2000. In Proceedings IGARSS 2000. IEEE 2000 International, Volume: 3 , 2000